RSC Advances

PAPER

View Article Online
View Journal | View Issue

Cite this: *RSC Adv.*, 2016, **6**, 76773

Morphological and crystallinity differences in nitrogen-doped carbon nanotubes grown by chemical vapour deposition decomposition of melamine over coal fly ash†

Lerato Hlekelele,[ab] Paul J. Franklyn,[b] Pranav K. Tripathi[ab] and Shane H. Durbach*[ab]

Millions of tons of coal fly ash (CFA) are produced each year in thermoelectric coal powered stations as a waste-product. Until recently few researchers have endeavored to use CFA as a catalyst in the formation of carbon nanomaterials (CNMs). In this study a two-stage tube furnace was used to synthesize N-doped carbon nanotubes (NCNTs) by chemical vapor deposition using melamine as the source of nitrogen and carbon, with CFA as a catalyst, at temperatures ranging from 800 to 900 °C. The masses of the NCNTs formed were found to have increased with increased synthesis temperature. The morphology and crystallinity of the NCNTs along with the amount of nitrogen incorporated into these were found to vary with the synthesis temperature. NCNTs synthesized at 800 °C were found to be typical multiwalled carbon nanotubes by transmission electron microscopy, whereas those at 850 and 900 °C were found to be chain-like and bamboo-like compartmentalised nanotubes respectively. The NCNTs synthesized at 800 °C were found to contain the least incorporation of nitrogen by elemental analysis and were the most crystalline (as determined by using the I_G/I_D ratio and the G-band position from laser Raman spectroscopy), whereas those at 850 °C were the least crystalline but had the highest incorporation of nitrogen. NCNTs synthesised at 800 °C were the most thermally stable, whereas those synthesized at 850 °C were the least stable. NCNTs synthesized at 900 °C had a crystallinity, thermal stability and nitrogen content which lay between the other two.

Received 30th June 2016
Accepted 7th August 2016

DOI: 10.1039/c6ra16858b

www.rsc.org/advances

Introduction

Coal fly ash (CFA) is an industrial by-product that is generated during the combustion of ground coal in thermoelectric coal powered stations.[1,2] Inorganic minerals form the major part of CFA, accounting for 90–99% of its matrix, whereas organic and fluid components account for 1–9% and 0.5% respectively.[3–5] CFA is a powdery material consisting of mainly spherically-shaped porous solid and hollow aluminosilicates particles.[5] The chemical composition of CFA consists of inorganic oxides such as: silica, alumina, haematite, lime, magnesium oxide, potassium oxide and titania amongst others.[3–6] The reclamation of CFA is vital because of the 800 Mt of CFA produced globally each year only 25% is reused, with the rest being disposed of in landfills and ash ponds.[7]

Several researchers have demonstrated that CFA can be used in catalysis.[3,8–12] For instance Xiaoping Xuan *et al.* investigated the selective catalytic reduction of NO with NH_3 using Fe, V, Ni and Cu supported on CFA.[8] CFA has also been shown to be a visible light photocatalyst and has been used to degrade 60% of 0.1 mM thionine solution in 4 h.[9] However, few reports on the synthesis of carbon nanomaterials (CNMs) from CFA have been made. Dunens *et al.* reported on the fixed bed catalytic chemical vapour deposition (CVD) synthesis of undoped carbon nanotubes (CNTs) through the decomposition of acetylene on Fe-impregnated CFA.[10] On the other hand, various undoped carbon nanomaterial morphologies: ropes, branches, whiskers and graphene sheets have been observed when polyvinyl alcohol and fly ash films were subjected to pyrolysis at 500 °C for 10 min in a nitrogen atmosphere.[11] Carbon nanofibers (CNFs) have been synthesized in our group by the decomposition of acetylene on fly ash in a reducing gas atmosphere by CVD.[12] Likewise we have shown that the yields of CNFs could be enhanced by pre-treating CFA with CO_2 before the introduction of C_2H_2 and H_2.[13] Saudi Arabian and Japanese CFA have also been used to synthesize undoped CNTs.[14,15] Similarly, Salah *et al.* have optimised the synthesis parameters (temperature, gas pressure, growth times, and gas flow rates for the

[a]*DST-NRF Centre of Excellence in Strong Materials, University of the Witwatersrand (Wits), Private bag X3, Johannesburg 2050, South Africa. E-mail: Shane.Durbach@wits.ac.za*

[b]*Molecular Sciences Institute, School of Chemistry, University of the Witwatersrand (Wits), Private bag X3, Johannesburg 2050, South Africa*

† Electronic supplementary information (ESI) available. See DOI: 10.1039/c6ra16858b

decomposition of C_2H_2 in the presence of H_2) for the growth of undoped MWCNTs on carbon rich CFA by low pressure chemical vapour deposition (LPCVD).[14] However, to date the synthesis of heteroatom-doped (*i.e.* nitrogen, phosphorus, sulphur or boron) CNTs over waste CFA has not been reported.

Since the rediscovery of carbon nanotubes (CNTs) by Iijima in 1991,[16] a great deal of research has been focused on fine-tuning the chemical properties of CNTs for various applications. One method which has been employed has been the manipulation of the chemical properties of CNTs by doping them with heteroatoms such as nitrogen and boron.[17] For instance, NCNTs have been shown to have a strong affinity to metals, which has resulted in good dispersion of metal nanoparticles on their surfaces for applications in catalysis.[18] The optical and electronic properties of CNTs have also been improved by N-doping.[19]

Although there has been some benefit in doping CNMs with other heteroatoms such as: phosphorus, sulphur and boron, doping with nitrogen has offered advantages that were not observed with these other dopants. For example, the electrochemical activity of NCNTs was found to have improved when used as metal-free electrocatalysts for oxygen reduction reactions.[20,21] This improved activity was attributed to the net positive charge on the carbon atoms, which was created by the dopant nitrogen atoms that had higher electronegativities than their carbon neighbours.[21] The other common heteroatom dopants (*i.e.* phosphorus and boron) have lower electronegatives relative to carbon atoms, thus this effect is almost exclusive to nitrogen dopants. Furthermore, nitrogen has been doped into carbon nanostructures in different configurations, *i.e.* pyridinic, quaternary and pyrrolic.[19,22,23] Indeed, it has been shown that pyridinic-N substituents had localized lone pairs which were active in base catalysed reactions, which is an advantage that has not been observed with other heteroatom doped CNMs.[19]

To achieve N-doped CNMs, chemicals such as: pyridine, aniline, ammonia, melamine and acetonitrile, amongst others have been used as precursors for the synthesis of NCNTs.[24,25] In this study, melamine was used as a lone carbon and nitrogen source as it is an organic molecule which has 67% nitrogen by mass, similar to that of carbon nitride (C_3N_4).[26]

Low-cost production of NCNTs is a desirable prospect as the current methodologies require the use of expensive precursors and catalysts. Since the cost of melamine is relatively low and fly ash is practically free, this served as an opportunity to deal with both of the above-mentioned limitations. In this paper the two-stage CVD synthesis of NCNTs from melamine over CFA has been reported for the first time. Here the effects of synthesis temperature on the morphology, crystallinity, and amount of nitrogen incorporated into these NCNTs were also investigated.

Experimental

Synthesis

The CFA used for this study was obtained from the Electricity Supply Commission (ESCOM) of South Africa's Research and Innovation Centre in Rosherville (which they had collected from hoppers at the Duvha power station). This raw CFA was used without any chemical or physical pre-treatments. Analytical grade melamine (Sigma-Aldrich) was used as purchased.

In this study a two-stage furnace with separate temperature controllers was used for the CVD synthesis of NCNTs (Fig. 1). A mass 1 g of melamine was weighed into a quartz boat which was placed into a quartz reactor tube and then inserted in the middle of the first-stage furnace (Fig. 1). A second quartz boat containing a mass of 0.5 g of raw CFA was placed in the middle of the second-stage furnace (Fig. 1). Nitrogen gas was introduced into the quartz reactor tube through the inlet at a flow rate of 50 ml min^{-1} throughout the duration of the experiment. The second-stage furnace was initially heated, at a heating rate of 10 °C min^{-1}, to: 800, 850 or 900 °C for the three separate experiments. Once the second-stage furnace had reached its set temperature then the first-stage furnace (with melamine) was in all cases rapidly heated to 350 °C at 35 °C min^{-1}. CFA is an inhomogeneous material, as such small variances in these results were obtained. To overcome this, experiments were conducted in triplicate. Thus the results reported in this article were the best representation of these experiments. NCNTs were also synthesized under exactly the same conditions for comparison using a more traditional catalyst, 5% Fe@$CaCO_3$ instead of CFA. Calcium carbonate is one of the most commonly used catalyst supports (especially for catalysts like Fe and Co) for the synthesis of CNTs.[27,28] In order to make a fair comparison, Fe (5%) was wet-impregnated onto $CaCO_3$, as Fe was previously shown to be the active metal for the growth of CNMs on CFA under CVD conditions.

Characterization

The raw CFA and the carbonaceous products formed in the reaction between the raw CFA and melamine were characterized by using: transmission electron microscopy (TEM, FEI Tecnai G2 Spirit electron microscope at 120 kV), scanning electron microscopy (SEM, FEI NOVA nanolab 600 FIB/SEM), laser Raman spectroscopy (Jobin-Yvon T64000 Raman spectrometer, with the excitation wavelength of 514.5 nm), Fourier transform infrared spectroscopy (FTIR, Bruker Vector 22 FT-IR spectrometer) and thermogravimetric analysis (TGA, Perkin Elmer Pyris 1

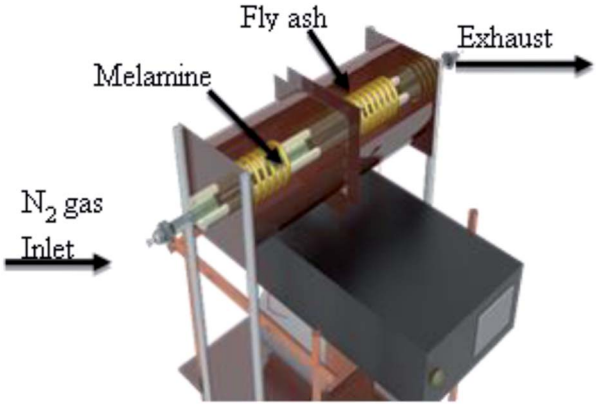

Fig. 1 Two-stage chemical vapour deposition set-up.

TGA). The amount of nitrogen incorporated in the carbonaceous materials was measured through CHNS analysis using a Carlo Erba EA 1108 Organic Elemental Analyzer. X-ray fluorescence spectroscopy (XRF, PANalytical PW2404 XRF spectrometer) and powder X-ray diffraction (PXRD, Bruker D2 PHASER diffractometer Ni-filtered Co Kα radiation), were also used in the analysis of the raw CFA and/or CFA after melamine decomposition.

Results and discussion

Data obtained by XRF spectroscopy showed that the raw CFA was pozzollanic (Table 1). According to the American Society for Testing Materials (ASTM C618), it was also classified as class F CFA because the concentration of: SiO_2, Al_2O_3 and Fe_2O_3 accounted for more than 70% of its composition.[5] XRF data also revealed modest amounts of Fe-related compounds (*i.e.* Fe_2O_3-0.57% and FeO-4.64%). For the purposes of this study this was desirable as minerals containing iron in CFA have previously been shown to be the active catalyst for the CVD synthesis of CNMs.[12] Silica and quartz were also identified using XRF spectroscopy and have been used as catalyst supports in the synthesis of CNTs using the CVD method.[29]

PXRD analysis of the raw CFA (Fig. 2(a)) indicated that its main mineralogical constituents were: quartz, mullite and haematite. Minor constituents, not highlighted in Fig. 2, consisted of oxides of: magnesium, potassium, titanium and sodium. The PXRD pattern of CFA after the decomposition of melamine showed a broad peak at the 28° 2θ position as highlighted on Fig. 2(b), which was indicative of the presence of carbonaceous products which had formed.

The morphology of CFA particles has usually been determined by the pyrolysis and cooling temperatures of coal.[4] SEM and TEM micrographs of the raw CFA revealed spherical particles, predominantly of silica and alumina, which had diameters that ranged between 1 and 15 μm (Fig. 3(a and b)).

Throughout these studies it was observed that the average masses of the carbonaceous products that were synthesized increased (*i.e.* 55, 112 and 310 mg) as the second-stage furnace temperature was increased (*i.e.* 800, 850 and 900 °C, respectively). This was attributed to the increased rate of decomposition of melamine on the CFA catalyst surface at higher temperatures. This was further qualified by thermogravimetric analysis (TGA), where it was observed that 60% of the products synthesized at 900 °C decomposed at temperatures between 30 and 900 °C, whereas 11 and 22% of the products synthesized at 800 and 850 °C respectively, decomposed (S1†). The percentage yield of the synthesized carbonaceous materials at various temperatures were calculated using eqn (1) (S2†). The highest yield was found for the product synthesized at 900 °C (44%), whilst experiments at 800 and 850 °C had percentage yields of 24 and 31% respectively. FTIR spectroscopy was used to characterise the carbonaceous products, where it was found that they were unlike CFA or the undecomposed melamine (S3†). Peaks at wavenumbers at 1445 cm^{-1} were associated with the CNTs, while those at 1385 cm^{-1} (N–CH_3), 1170 cm^{-1} (C–N) and 2188 cm^{-1} (C=N) were associated with nitrogen containing carbonaceous materials (suspected to be NCNTs).[30] These carbonaceous products were then characterised by TEM.

TEM analyses revealed that the carbonaceous materials synthesized at the various temperatures were tubular in morphology. For instance, the samples synthesized at 800 °C were found to be multiwalled carbon nanotubes (MWCNTs) (Fig. 4(a and b)) without bamboo compartments typical of NCNTs. This lack of bamboo compartmentalisation did not necessarily imply that nitrogen doping had not been achieved, as NCNTs have been formed without these when Ni and Co were used as the catalyst.[31] Similarly, at low N incorporation levels, this bamboo morphology was not observed even when Fe was used.[19] The CNTs synthesized at 800 °C had thick multiple walls with an average thickness of 13 nm, appeared crystalline

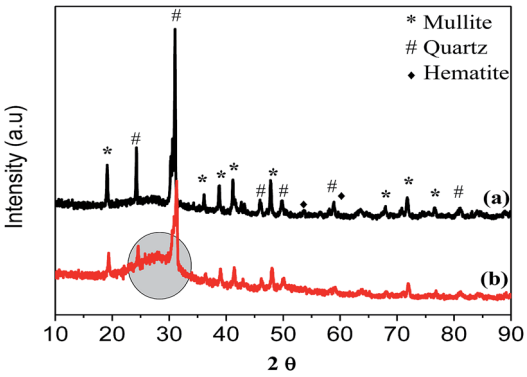

Fig. 2 PXRD pattern of the: (a) raw CFA and (b) CFA after the decomposition of melamine on its surface at 800 °C.

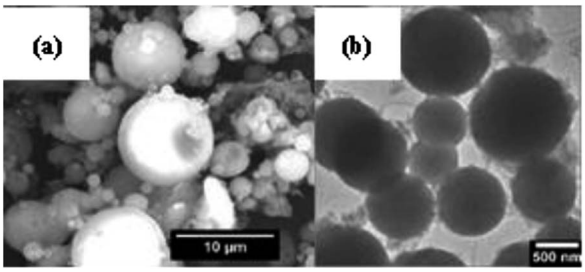

Fig. 3 (a) SEM micrograph and (b) TEM micrograph of raw CFA showing spherical particles with varying diameters.

Table 1 Composition of raw CFA as determined by XRF spectroscopy

Mineral	%/mass
SiO_2	58.14
Al_2O_3	28.79
Fe_2O_3	0.57
FeO	4.64
MnO	0.05
MgO	1.04
CaO	3.54
Na_2O	0.05
K_2O	0.77
TiO_2	1.57

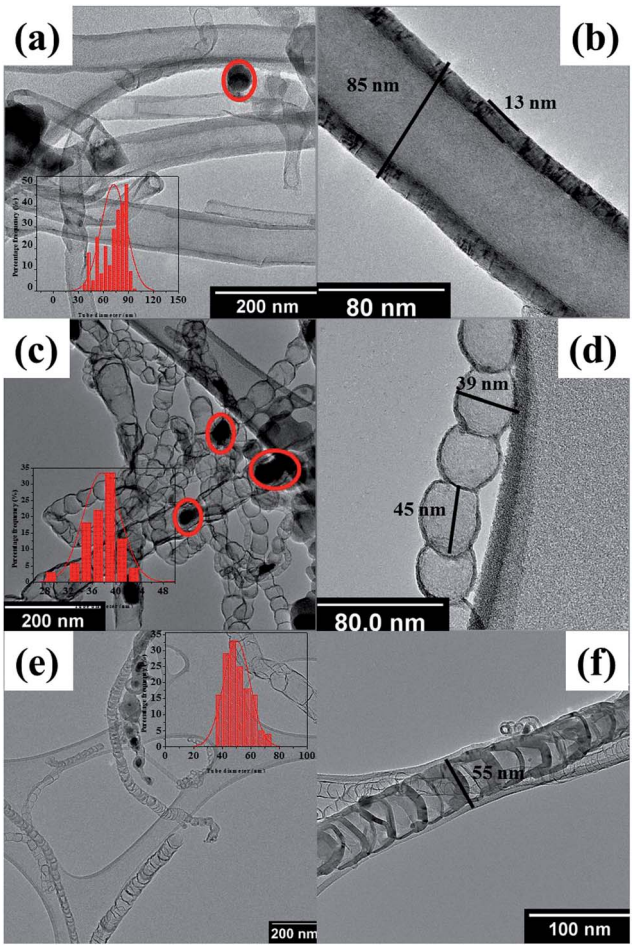

Fig. 4 (a) TEM image of carbonaceous materials synthesized at: (a and b) 800 °C, (c and d) 850 °C and (e and f) 900 °C.

and had diameters which ranged between 74 and 96 nm (Fig. 4(a and b)).

Differences in the morphologies of the CNTs synthesized at 850 and 900 °C were noted. The CNTs synthesized at 850 °C were found to have a morphology that could be likened to that of a chain that had circular hollow compartments strung together to form a tube (Fig. 4(c and d)). On the other hand, CNTs synthesized at 900 °C consisted of tubes with what appeared to be well-ordered walls and separate hollow cone-like bamboo compartments (Fig. 4(e and f)). Hao Liu *et al.* have observed similar morphological differences and attributed them to the amount of nitrogen incorporated into their cylindrical graphene materials.[23,32–34] The more irregular morphologies (formed as a consequence of nitrogen replacing carbon), which were less crystalline, were reported to have contained higher concentrations of nitrogen.[23,32–34] Likewise, Jang *et al.* showed that compartments like those seen in this study were attributable to the inclusion of C=N bonds in the graphene network.[32] Nxumalo *et al.* have also reported that the effects of nitrogen incorporation into the graphene network were more pronounced in the inner layers of such tubes *i.e.* their bamboo characteristics became more pronounced.[19] This was consistent with Jang *et al.* who showed that as the amount of nitrogen incorporated in the sp^2 graphene cylinders increased, the size of the bamboo compartments inside the tube decreased with increased number.[32] In our study both types of tubes synthesized at 850 and 900 °C had compartments which were typical of NCNTs, but the former had walls that were better spaced apart and appeared less crystalline than the latter. The tube diameters of CNTs synthesized at 850 °C ranged between 28 and 62 nm and their multiple walls (both side and inner compartmental walls) had an average thickness of 12 nm. In the case of CNTs synthesized at 900 °C, their tube diameters ranged between 32 and 75 nm and the average thickness of the multiple walls was 10 nm. Furthermore, clear morphological differences between the CNTs synthesized at different temperatures were observed by SEM (S4†).

As highlighted in the methodology section, the images discussed in Fig. 4 were a representation of the predominant (>80%) morphology that was observed. Images of the other variants are shown in S5.† The CNTs synthesized using Fe@$CaCO_3$ for comparison were also analysed using TEM (S6†). Morphological differences were observed between the CNTs synthesized using the two different catalysts at the same temperature. As in the case of CFA, the CNTs synthesized by Fe@$CaCO_3$ at various temperatures also had morphological variations. However, these did not include the chain-like CNTs shown in (Fig. 4(c and d)). Unlike the case with CFA, the CNTs grown from Fe@$CaCO_3$ were found to have much narrower tube diameter distributions. This was most likely due to the fact that Fe@$CaCO_3$ was a much more homogeneous catalyst than CFA.

The precise mechanism under which the CNTs were grown from CFA catalyst under 2-stage CVD conditions has not been fully established. However, in several instances (Fig. 2(a and c)) catalyst nanoparticles were observed inside and at the tips of the CNTs (circled in red), which meant that the tip-growth mechanism could not be disregarded.[12] Hintsho *et al.* showed that Fe_3C was the predominant Fe specie present after exposing this same kind of CFA to acetylene to grow CNFs.[12] Since Fe was present in the form of Fe_2O_3 and FeO in this CFA (Table 1), it is possible that upon the decomposition of melamine, the metastable Fe_3C also formed and led to the tip growth of CNTs. Indeed, several authors have reported tip-growth of nitrogen-doped CNTs from various catalysts.[35–37]

Elemental analysis is a rapid method in which a quantitative determination of carbon, hydrogen, nitrogen and sulphur (CHNS) in a sample can be determined. The CNTs synthesised under the various temperatures were analysed specifically for their weight percentage of nitrogen by this technique and the results are shown in Table 2.

Here it was observed that the CNTs synthesized at 850 °C contained the highest weight% N (*i.e.* 3.16%), followed by those synthesized at 900 °C (1.95%). CNTs synthesised at 800 °C

Table 2 Weight percentages of nitrogen in the CNTs synthesized at various temperatures as determined by elemental analysis

Temperature (°C)	800	850	900
% N (CFA as catalyst)	1.10	3.16	1.95
% N (Fe@$CaCO_3$ as catalyst)	5.55	6.53	10.92

contained the least weight% of N (*i.e.* 1.10%). This, together with the FTIR data and morphological evidence from TEM served as confirmation that the tubes which were formed were NCNTs.

A schematic conceptualising the differences in the morphology of the CNTs synthesized at the different temperatures is given in Fig. 5.

However, these results showed that there was no direct correlation between the % N that was incorporated into these NCNTs and the temperature at which they were grown on CFA, as might have been expected. Nonetheless, a correlation was drawn between the morphological features of the NCNTs synthesized at different temperatures and the amount of nitrogen incorporated. Here NCNTs which had the highest % N incorporated into them were observed to have the most "irregular morphologies". On the other hand NCNTs which had the least % N incorporated had morphologies that were closer to those of MWCNTs. When the NCNTs grown on Fe@$CaCO_3$ were analysed, not only was the % N incorporated higher than for the NCNTs grown from CFA, but it increased with increased temperature. Hence in order to establish whether the % N incorporated into these materials had affected their graphicity as they had their morphology, NCNTs from CFA and Fe@$CaCO_3$ were then further analysed by laser Raman spectroscopy.

Laser Raman spectroscopy has been demonstrated to be a useful technique for studying the irregularities and crystallinity of graphene-based materials. The Raman spectra of the NCNTs that were synthesized under different temperatures over CFA are shown in Fig. 6.

In these spectra the strong bands in the region of 1350 cm^{-1} were assigned as the D-bands, which have been reported to have arisen as a result of defects in graphene-based materials and have been affiliated with optical phonons close to the *K*-point of their Brillouin zone.[38] The bands that were observed in the region of 1580 cm^{-1} were denoted as the G-bands, which were Raman allowed and associated with the optical phonon modes of the E_{2g} symmetry in graphene-based materials.[39]

The integration of the normalized D and G-bands, to give an intensity ratio *i.e.* I_G/I_D, has been found to be dependent on the defects present in carbon nanomaterials and has therefore been used to measure their crystallinity and defect-density.[40] The

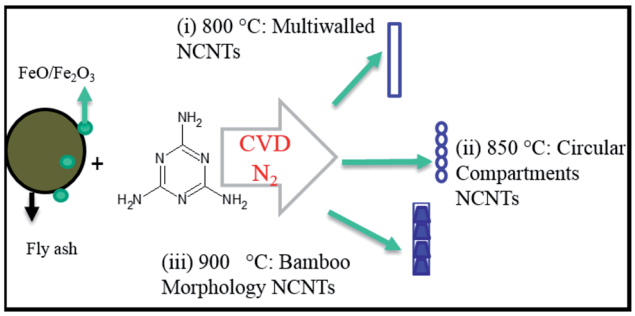

Fig. 5 Schematic of reactions conducted at: (i) 800 °C where multi-walled NCNTs were formed, (ii) 850 °C where NCNTs with circular compartments were formed and (iii) 900 °C where NCNTs with typical bamboo morphology were formed.

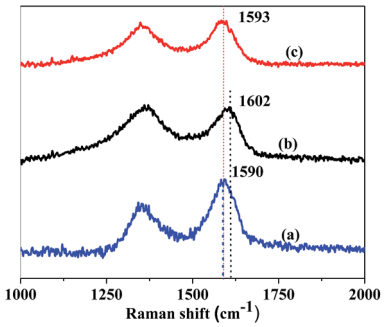

Fig. 6 Laser Raman spectra for NCNTs synthesized from CFA at: (a) 800 °C, (b) 850 °C and (c) 900 °C.

incorporation of nitrogen into the lattice of graphene-based materials is known to have resulted in the formation of defects in their structures.[18] Hence this made it possible to use laser Raman spectroscopy to measure the crystallinity, as well as to estimate the extent of nitrogen incorporation in the NCNTS formed in this study. The I_G/I_D ratios of the NCNTs grown from CFA at different temperatures were plotted in Fig. 7.

The NCNTs synthesized at 800 °C had the highest I_G/I_D ratio which indicated that they had the least defects *i.e.* were the most crystalline. Comparing NCNTs synthesized at 850 °C and 900 °C, the I_G/I_D ratio of the NCNTs synthesized at 850 °C was found to be the lowest, while the NCNTs synthesized at 900 °C had an I_G/I_D ratio that was intermediate relative to the other two. Based upon these ratios, these results suggested that the crystallinity of the NCNTs decreased as the % N incorporated increased. The Raman results were found to be consistent with the data obtained by elemental analysis of the NCNTs grown from CFA (Table 2). Significantly these results were consistent with those of Liu *et al.* who observed that the I_D/I_G ratio increased (*i.e.* I_G/I_D ratio decreased) with increased % N incorporated in the NCNTs that were formed when a floating catalyst system was used with melamine as the nitrogen source.[34] The I_G/I_D ratios of NCNTs grown from Fe@$CaCO_3$ were found to be lower than those of NCNTs grown from CFA (S7†) and were consistent with the CHNS results (Table 2).

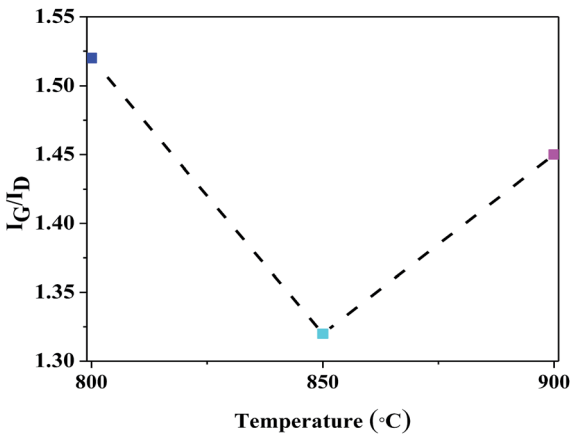

Fig. 7 Plots of the intensity of the G-band (1590 cm^{-1}) and D-band (1340 cm^{-1}) ratio for NCNTs grown from CFA.

Furthermore, in this present study, the G-bands for NCNTs from CFA appeared to reach a maximum and then decrease in wavenumber (*i.e.* from 1590 cm^{-1} to 1602 cm^{-1} and then back down to 1593 cm^{-1}) with increased % N incorporated (*i.e.* from 1.1% to 3.16% and then back down to 1.95%) (Fig. 6 and Table 2), for the NCNTs that were synthesized at the various temperatures. Concomitantly as this wavenumber shift occurred the morphology of these products changed from tubes (most crystalline) to chain-like structures (least crystalline) and back to tubes which were compartmentalised (intermediate crystallinity).

Shifts in laser Raman peaks, in relation to the % N incorporated into a carbon network, have been reported to have taken place due to charge-transfer from the nitrogen dopants to the carbon.[41] However, in contrast to the results in our study Liu *et al.* have noted a shift to lower wavenumbers in the G-band as the % N incorporated into the graphene structure increased.[34] Three possible explanations could be postulated for this variance: the first is that Liu *et al.* performed their experiments at a fixed temperature (while the reaction temperature was varied in our study and did not reach 950 °C); the second is that ethylene and melamine were used in their study (while only melamine was used in our study); the third was that varying masses of melamine were used in their study (while a fixed mass of melamine was used in our study).

The thermal stabilities of different types of carbon nanomaterials can be evaluated using TGA in oxygen. Fig. 8 is a TGA derivative profile of the various NCNTs that were grown at different temperatures from CFA. Here it was observed that the NCNTs that were grown at 850 °C started decomposing at a lower temperature, followed by the NCNTs synthesized at 900 and 800 °C respectively.

The data obtained from the TGA revealed that as the % N incorporated in the NCNTs increased (*i.e.* from 1.1% to 3.16%), the decomposition temperature at which these materials burned decreased (*i.e.* from 520 °C to 440 °C). This observation was consistent with Villalpando-Paez *et al.*, who showed that the decomposition temperature of NCNTs decreased when the % N incorporated in these materials increased.[42] In contrast with the NCNTs grown from CFA, where only one major decomposition peak was observed (between 440 and 520 °C) in the TGA derivative profiles, in the case of NCNTs grown from Fe@$CaCO_3$ two separate decomposition peaks were observed. The first was for the NCNTs (between 450 and 550 °C) and the second for the $CaCO_3$ support (between 700 and 750 °C) which burnt off at a significantly higher temperature (S8†). Unlike the NCNTs grown from CFA, the peaks in the TGA derivative profiles for NCNTs grown from Fe@$CaCO_3$ shifted to higher temperatures as the % N incorporated in these materials increased.

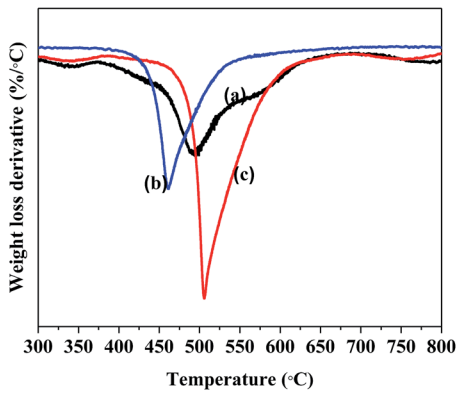

Fig. 8 TGA derivative profiles of NCNTs grown from CFA at: (a) 800 °C, (b) 850 °C and (c) 900 °C.

Conclusions

The decomposition of melamine on the surface of raw CFA, in the presence of nitrogen gas under CVD conditions, to form useful nitrogen-doped carbon nanomaterials was presented in this study. Here the reaction temperature was varied (from 800 to 900 °C) where it was observed that the mass of NCNTs formed increased with increased reaction temperature. It was also demonstrated that the reaction temperature influenced the: morphology, crystallinity and the wt% of N incorporated into the NCNTs. The data revealed through laser Raman spectroscopy, TGA and elemental analyses, that NCNTs synthesized at 850 °C were the least crystalline and contained the most nitrogen. On the other hand, NCNTs synthesized at 800 °C were shown to be the most crystalline and contained the least wt% of N, followed by NCNTs synthesized at 900 °C. NCNTs grown from CFA were noted to have been formed by tip-growth at the various synthesis temperatures. Furthermore this study has shown that the quality of the NCNTs grown from the waste CFA and synthesised Fe@$CaCO_3$ catalysts was similar. However, two main variances were noted when the CFA and Fe@$CaCO_3$ catalysts were used. The first was that NCNTs grown from Fe@$CaCO_3$ were predominantly the same kind, irrespective of reaction temperature, with a narrow diameter distribution. The second was that different types of NCNTs were formed when CFA was used as a catalyst and in particular chain-like NCNTs could be grown which were not observed when Fe@$CaCO_3$ was used. This latter observation has shown that CFA could be a more versatile catalyst, should different types of NCNTs be required for various applications. Although large-scale synthesis of NCNTs using this procedure has not been fully demonstrated, this study has opened up the field to the use of waste solids (like CFA) as catalysts in the lower-cost synthesis of such materials.

Acknowledgements

This work is based on the research supported in part by the National Research Foundation of South Africa (Grant number 88076), ESCOM's Tertiary Education Support Programme (TESP) and the DST-NRF Centre of Excellence in Strong Materials (CoE-SM) at the University of the Witwatersrand. The authors would also like to thank the staff in the Microscopy and Microanalysis Unit (MMU) at the University of the Witwatersrand for assisting with the SEM and TEM analyses, Dr R Erasmus based in the Raman and Luminescence Laboratory at the University of the Witwatersrand, as well as Prof Rui Krause for the CHNS elemental analyses at Rhodes University.

References

1 L. F. O. Silva, A. Jasper, M. L. Andrade, C. H. Sampaio, S. Dai, X. Li, T. Li, W. Chen, X. Wang, H. Liu, L. Zhao, S. G. Hopps, R. F. Jewell and J. C. Hower, *Sci. Total Environ.*, 2012, **419**, 250–264.
2 I. Kostova, C. Vassileva, S. Dai, J. C. Hower and D. Apostolova, *Int. J. Coal Geol.*, 2013, **116–117**, 227–235.
3 S. V. Vassilev and C. G. Vassileva, *Energy Fuels*, 2005, **19**, 1084–1098.
4 R. S. Blissett and N. A. Rowson, *Fuel*, 2012, **97**, 1–23.
5 M. Ahmaruzzaman, *Prog. Energy Combust. Sci.*, 2010, **36**, 327–363.
6 M. Basu, M. Pande, P. B. S. Bhadoria and S. C. Mahapatra, *Prog. Nat. Sci.*, 2009, **19**, 1173–1186.
7 D. Panias, I. P. Giannopoulou and T. Perraki, *Colloids Surf., A*, 2007, **301**, 246–254.
8 X. Xuan, C. Yue, S. Li and Q. Yao, *Fuel*, 2003, **82**, 575–579.
9 D. Chatterjee, B. Ruj and A. Mahata, *Catal. Commun.*, 2001, **2**, 113–117.
10 O. M. Dunens, K. J. MacKenzie and A. T. Harris, *Environ. Sci. Technol.*, 2009, **43**, 7889–7894.
11 D. C. D. Nath and V. Sahajwalla, *Appl. Phys. A*, 2011, **104**, 539–544.
12 N. Hintsho, A. Shaikjee, H. Masenda, D. Naidoo, D. Billing, P. Franklyn and S. Durbach, *Nanoscale Res. Lett.*, 2014, **9**, 387.
13 N. Hintsho, A. Shaikjee, P. Franklyn and S. Durbach, *RSC Adv.*, 2015, **5**, 53776–53781.
14 N. Salah, A. A. Al-ghamdi, A. Memic, S. S. Habib and Z. H. Khan, *Mater. Manuf. Processes*, 2016, **31**, 146–156.
15 A. Yasui, Y. Kamiya, S. Sugiyama, S. Ono, H. Noda and Y. Ichikawa, *IEEJ Trans. Electr. Electron. Eng.*, 2009, **4**, 787–789.
16 S. Iijima, *Nature*, 1991, **354**, 56–58.
17 K. Ghosh, M. Kumar, T. Maruyama and Y. Ando, *Carbon*, 2010, **48**, 191–200.
18 S. R. Stoyanov, A. V. Titov and P. Kral, *Coord. Chem. Rev.*, 2009, **253**, 2852–2871.
19 E. N. Nxumalo and N. J. Coville, *Materials*, 2010, **3**, 2141–2171.
20 Y. Dingshan, X. Yuhua and L. Dai, *J. Phys. Chem. Lett.*, 2012, **3**, 2863–2870.
21 K. P. Gong, F. Du, Z. H. Xia, M. Durstock and L. Dai, *Science*, 2009, **323**, 760–764.
22 H. Wang, T. Maiyalagan and X. Wang, *ACS Catal.*, 2012, **2**, 781–794.
23 P. Ayala, R. Arenal, M. Rümmeli, A. Rubio and T. Pichler, *Carbon*, 2010, **48**, 575–586.
24 X. Wang, X. Li, L. Zhang, Y. Yoon, P. K. Weber, H. Wang, J. Guo and H. Dai, *Science*, 2009, **324**, 768–771.
25 C. P. Ewels and M. Glerup, *J. Nanosci. Nanotechnol.*, 2005, **5**, 1345–1363.
26 H. Montigaud, B. Tanguy, I. Gérard Demazeau, M. B. Alves and J. Dunogues, *Mater. Sci. Forum*, 2000, **325**, 31–36.
27 A. Magrez, J. W. Seo, R. Smajda, M. Mionić and L. Forró, *Materials*, 2010, **3**, 4871–4891.
28 E. Dixon Dikio and N. D. Shooto, *Chem. Sci. Trans.*, 2013, **2**, 1160–1173.
29 Q. W. Li, X. F. Zhang, R. F. DePaula, L. X. Zheng, Y. H. Zhao, L. Stan, T. G. Holesinger, P. N. Arendt, D. E. Peterson and Y. T. Zhu, *Adv. Mater.*, 2006, **18**, 3160–3163.
30 A. Misra, P. K. Tyagi, M. K. Singh and D. S. Misra, *Diamond Relat. Mater.*, 2006, **15**, 385–388.
31 A. G. Kudashov, A. V. Okotrub, L. G. Bulusheva, I. P. Asanov, Y. V. Shubin, N. F. Yudanov, L. I. Yudanova, V. S. Danilovich and O. G. Abrosimov, *J. Phys. Chem. B*, 2004, **108**, 9048–9053.
32 J. W. Jang, C. E. Lee, S. C. Lyu, T. J. Lee and C. J. Lee, *Appl. Phys. Lett.*, 2004, **84**, 2877.
33 K. Chizari, A. Vena, L. Laurentius and U. Sundararaj, *Carbon*, 2014, **68**, 369–379.
34 H. Liu, Y. Zhang, R. Li, X. Sun, S. Désilets, H. Abou-Rachid, M. Jaidann and L.-S. Lussier, *Carbon*, 2010, **48**, 1498–1507.
35 M. Nath, B. C. Satishkumar, A. Govindaraj, C. P. Vinod and C. N. R. Rao, *Chem. Phys. Lett.*, 2000, **322**, 333–340.
36 T. Sharifi, F. Nitze, H. R. Barzegar, C.-W. Tai, M. Mazurkiewicz, A. Malolepszy, L. Stobinski and T. Wågberg, *Carbon*, 2012, **50**, 3535–3541.
37 J. P. O'Byrne, Z. Li, S. L. T. Jones, P. G. Fleming, J. A. Larsson, M. A. Morris and J. D. Holmes, *ChemPhysChem*, 2011, **12**, 2995–3001.
38 S. Wang, *Environ. Sci. Technol.*, 2008, **42**, 7055–7063.
39 R. M. Yadav, P. S. Dobal, T. Shripathi, R. S. Katiyar and O. N. Srivastava, *Nanoscale Res. Lett.*, 2008, **4**, 197–203.
40 R. Czerw, M. Terrones, J. Charlier, X. Blase, B. Foley, M. Ru and D. L. Carroll, *Nano Lett.*, 2001, **1**, 457–460.
41 S. Lim, H. Elim, X. Gao, a. Wee, W. Ji, J. Lee and J. Lin, *Phys. Rev. B: Condens. Matter Mater. Phys.*, 2006, **73**, 045402.
42 F. Villalpando-Paez, A. Zamudio, A. L. Elias, H. Son, E. B. Barros, S. G. Chou, Y. A. Kim, H. Muramatsu, T. Hayashi, J. Kong, H. Terrones, G. Dresselhaus, M. Endo, M. Terrones and M. S. Dresselhaus, *Chem. Phys. Lett.*, 2006, **424**, 345–352.